Comparison of Fully Distributed and Periodically Loaded Nonlinear Transmission Lines

Jean-Marc Duchamp, Philippe Ferrari, M. Fernandez, A. Jrad, Xavier Mélique, Junwu Tao, S. Arscott, Didier Lippens, and R. G. Harrison, *Member, IEEE*

***Abstract*—Two different approaches to realizing nonlinear transmission lines (NLTLs) are investigated in detail. In the first approach, the nonlinearity is continuously distributed along the line; in the second, the line is periodically loaded (PL) with discrete nonlinear elements. Measured heterostructure-barrier varactor (HBV) characteristics are used as the nonlinearities in both pulse-compression and harmonic-generation (20–60-GHz tripler) simulations. We point out that the choice of simulation step size is critical in the case of fully distributed (FD) NLTLs, and should be made sufficiently small that no numerical Bragg cutoff frequency appears. For the frequency tripler considered in this paper, simulations show that with PL (PL) NLTLs, 21% efficiency at 210-mW output power and 30% bandwidth can be obtained, whereas only 4.8% efficiency is possible using FD NLTLs. For pulse compression, we find that when properly matched, the FD NLTLs can deliver pulses that are five times sharper than can be obtained with the PL NLTLs. Measured results for an HBV-based PL NLTL frequency multiplier are reported that agree with our simulations, in particular, the 30% bandwidth. The confirmation of the role of the Bragg cutoff frequency in preventing the generation and propagation of undesired harmonics (this improving the conversion efficiency) is obtained from experimental results carried out from hybrid Schottky diodes NLTL measurements.**

***Index Terms*—Harmonic generation, heterojunctions, transmission-line circuits, varactor.**

I. Introduction

DUE TO technological progress in fast integrated Schottky diodes, practical nonlinear transmission lines (NLTLs) with excellent performance have been realized in the past decade. Major applications include ultrashort pulse generation in fast sampling systems and harmonic generation in large-bandwidth multipliers [1], [2]. The use of heterostructure-barrier varactors (HBVs) in NLTLs has been first investigated in [3] for pulse compression and harmonic generation. Recently, HBVs have been used to realize a frequency tripler with 130-GHz output frequency, based on a hybrid NLTL [4]. In all published realizations, a periodically loaded (PL) NLTL approach has been used, i.e., a linear transmission line is PL by nonlinear devices, either Schottky or HBV diodes.

However, fully distributed (FD) NLTLs offer an interesting alternative approach. The drawbacks of FD NLTLs based on microstrip structures with Schottky diodes were noticed as early as 1977 in [5], which underlined the problem of undesirable harmonic generation, and in 1987, by Rodwell [6], who discussed diode losses at high frequencies and geometrical problems in realizing matched NLTLs. Nevertheless, FD NLTLs have advantages, as well as drawbacks. Not only are the distributed structures simpler to fabricate, but the NLTLs are much shorter, partly compensating for the increased losses. Furthermore, FD NLTLs based on HBVs have not yet been completely studied. Finally, recently published simulation results [7] show interesting results for a FD NLTL. For all these reasons, it has been difficult to answer the simple question: "Are the FD NLTLs promising, and if so, for what kinds of applications?"

Based on SPICE simulations, this paper compares the behavior of PL and FD NLTLs in pulse-compression and frequency-multiplier applications. First, we describe the models used in this study for the HBV diodes fabricated by the Institut d'Electronique de Microélectronique et de Nanotechnologie (IEMN), Villeneuve d'Ascq, France [8]. These HBVs, presented in Section II, show very good performance with a $C_{\max}/C_{\min}$ ratio of $5:1$. In Section II, we then focus on the choice of the simulation step when dealing with FD NLTLs. We take care to point out that, in repeating the simulations published in [7], a "numerical" Bragg cutoff frequency can appear if the step size is not correctly chosen. Simulation results obtained with measured HBV voltage variable capacitance characteristics show that PL NLTLs using HBV diodes lead to efficient frequency triplers, whereas FD NLTLs exhibit poor results as triplers, although they can provide sharp-edged "sawtooth" waveforms similar to those produced by a van der Pol (vdP) oscillator in relaxation mode. We report measured results for an HBV-based PL NLTL frequency multiplier. Even though it does not correspond to the optimal simulated NLTL, the results agree with our simulations, in particular, the 30% bandwidth.

As pulse sharpeners, simulations show that appropriately matched FD NLTLs with sufficiently low losses can produce pulses with rise times five times faster than what is possible with PL NLTLs.

To validate our simulation-based theoretical studies of PL-FDs, we have realized hybrid Schottky-diode NLTLs. Experimental results on these NLTLs agree with simulations and confirm the role of the Bragg cutoff frequency in preventing the generation and propagation of undesired harmonics.

Manuscript received March 20, 2002; revised November 25, 2002.

J.-M. Duchamp and P. Ferrari are with the Laboratoire d'Hyperfréquences et de Caractérization, Université de Savoie, 73376 Savoie, France

M. Fernandez, X. Mélique, S. Arscott, and D. Lippens are with the Institut d'Electronique, de Microélectronique et de Nanotechnologie, Université des Sciences et Technologies de Lille, 59655 Lille, France.

A. Jrad is with the Laboratoire de Physique Appliquée, Faculté des Sciences III, Université Libanaise BP, 14-6573 Liban, France.

J. Tao was with the Laboratoire d'Hyperfréquences et de Caractérization, Université de Savoie, 73376 Savoie, France. He is now with the ENSEEIHT—INPT, National Polytechnique of Toulouse, 31071 Toulouse, France.

R. G. Harrison is with the Department of Electronics, Carleton University, Ottawa, ON, Canada K1S 5B6.

Digital Object Identifier 10.1109/TMTT.2003.809621

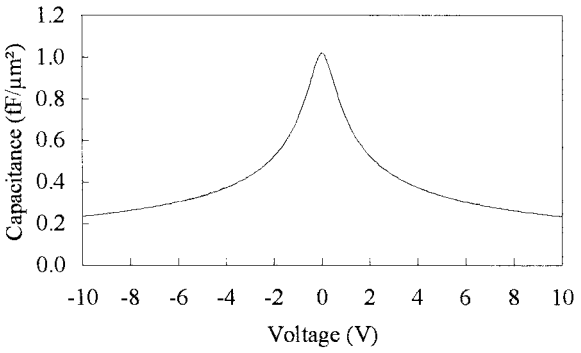

Fig. 1. $C(V)$ characteristic of the HBVs.

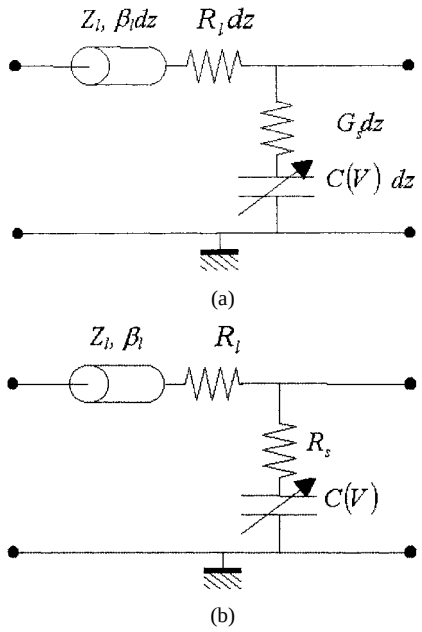

Fig. 2. NLTL equivalent-circuit models for an elementary section. (a) PL. (b) FD.

II. Theoretical Background—Models

FD and PL NLTLs use the same nonlinear effect. For PL NLTLs, the nonlinear elements are lumped, whereas the active region is distributed all along the transmission line for FD NLTLs. Fig. 1 gives the measured $C(V)$ characteristic for the HBVs realized at IEMN [8]. For these HBV, the active epilayer consists of two barriers integrated in series during the epitaxial growth, leading to a 10-V breakdown voltage.

The equivalent-circuit models for PL and FD NLTLs are given in Fig. 2.

For PL NLTLs, the parameters of the model are related to each elementary section. Z_l, β_l, and R_l are, respectively, the linear transmission-line characteristic impedance, propagation constant, and series resistance (representing metallic losses). R_s is the HBV diode series resistance.

For FD NLTLs, per-length parameters are used; dz is the step used for the simulations. As in [7], by using the model of Fig. 2(b), we assume that FD NLTLs can be modeled as linear transmission lines with superimposed nonlinear effects. That means we consider a quasi-static model. This is correct if the discretization step is small compared to the wavelength corresponding to the Bragg frequency, which is a realized condition. As demonstrated below, dz must be small enough for the simulations to give reliable results. We can then replace the linear transmission line by its per-length equivalent inductance L_l and capacitance C_l. Usually, C_l is very small compared with $C(V)$ and can be neglected.

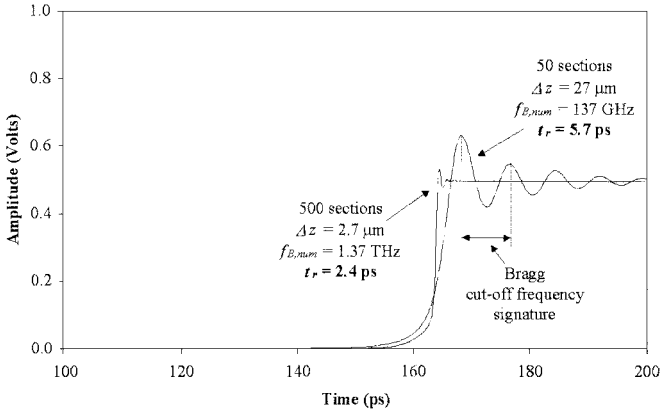

Fig. 3. Simulation of the pulse compression detailed in [7, Fig. 11].

III. Simulations

For PL NLTLs, various simulation methods have been used in the past, including harmonic balance, SPICE, finite difference time domain (FDTD), numerical integration, and others. This point no longer constitutes a problem. We have used harmonic-balance and SPICE approaches and find the same results. All the simulations in this paper have been achieved with SPICE.

A. Simulation Step Size for FD NLTLs

The simulation of FD NLTLs has not previously been explored completely. For the simulation, dz becomes discrete and is written Δz. The FD NLTL discretization leads to the appearance of a numerical Bragg frequency

$$f_{B,\mathrm{num}} = \frac{1}{\pi\sqrt{L1\Delta z C_{\mathrm{ls}}\Delta z}} = \frac{1}{\pi\Delta z\sqrt{L1C_{\mathrm{ls}}}} \tag{1}$$

where C_{ls} is the NLTL large signal per-length capacitance defined by

$$C_{\mathrm{ls}} = \frac{1}{V_{\max} - V_{\min}} \int_{V_{\min}}^{V_{\max}} C(v) \cdot dv. \tag{2}$$

If the discretization step Δz is too large, then the numerical Bragg frequency will be too small. This will affect the simulations, leading to unreliable results. For pulse compression, Fig. 3 shows results obtained for the NLTL of length 1.35 mm used by Li *et al.* [7]. This FD NLTL was cut into 50 elementary sections, leading to a step Δz equal to 27 μm. We compare this with a step of 2.7 μm, leading to 500 elementary sections.

For 50 sections, the results published in [7] are obtained, with a rise time of $t_r = 5.7$ ps and an overshoot of 23%. For 500 sections, $t_r = 2.4$ ps and the overshoot is 8%.

These results, though disturbing *a priori*, are simply explained by the problem of the numerical Bragg frequency $f_{B,\mathrm{num}}$.

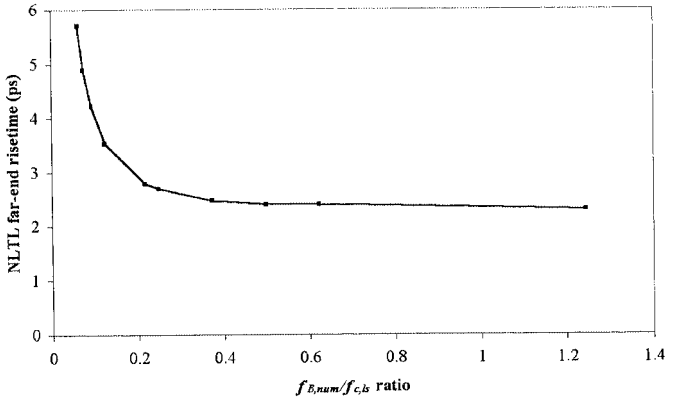

Fig. 4. Far-end NLTL rise time versus the ratio between the numerical Bragg and physical cutoff frequencies.

For the 50-section FD NLTL of Fig. 3, $f_{B,\mathrm{num}}$ is 137 GHz. This cutoff frequency is smaller than the NLTL large-signal cutoff frequency

$$f_{c,\mathrm{ls}} = \frac{1}{2\pi\left(\frac{R_s}{dz}\right)C_{\mathrm{ls}}dz} = \frac{1}{2\pi R_s C_{\mathrm{ls}}} = 2.2\ \mathrm{THz}. \quad (3)$$

Note that $f_{c,\mathrm{ls}}$ does not depend on dz. This numerical Bragg frequency phenomenon explains the oscillations (which constitute a signature of the Bragg frequency filtering effect) and the apparent degradation of the rise time with 50 sections. To determine how the simulation step should be chosen to avoid this problem, a convergence study on the rise time has been carried out. Fig. 4 shows the far-end NLTL rise time versus the ratio $f_{B,\mathrm{num}}/f_{c,\mathrm{ls}}$ and shows that substantial convergence is achieved when the condition $f_{B,\mathrm{num}} > f_{c,\mathrm{ls}}/4$ is respected.

With this criterion, the simulation error associated with the NLTL far-end pulse rise time is less than 5% for all the NLTLs we have simulated. It is surprising that even when $f_{B,\mathrm{num}} < f_{c,\mathrm{ls}}$, accurate results are still obtained. A similar effect, also due to a numerical Bragg cutoff frequency, can be seen when dealing with harmonic generation. Fig. 5(a) shows the results obtained for the tripler simulated in [7, Fig. 6(a)] for 50 and 500 sections.

The NLTL far-end waveforms are completely different in the two cases. The third harmonic is very small if the simulation step is correctly chosen. We find a harmonic amplitude of 60 mV instead of approximately 220 mV, as in [7]. Fig. 6 shows the harmonics obtained for 50 and 500 sections. It is seen that the FD NLTL exhibits higher power for harmonics above the fifth (corresponding to a quintupler). In this way, the results for pulse compression and harmonic generation can be simply explained. For pulse compression, $f_{B,\mathrm{num}}$ constitutes a limit to harmonic spreading, leading to an overestimated rise time, and the occurrence of oscillations. On the other hand, for harmonic generation, the energy is concentrated in the harmonics below the numerical Bragg frequency, leading to an overestimation of the third or fifth harmonic generation.

The tripler waveform in Fig. 5(a) obtained for the 500-section simulation is remarkably similar to that of a generalized vdP oscillator operating in the "relaxation" regime [see Fig. 5(b)]. What is interesting is that both the HBV–NLTL tripler simulated in [7] and the vdP oscillator involve pure-cubic nonlinearities. This is discussed in more detail in Appendix II.

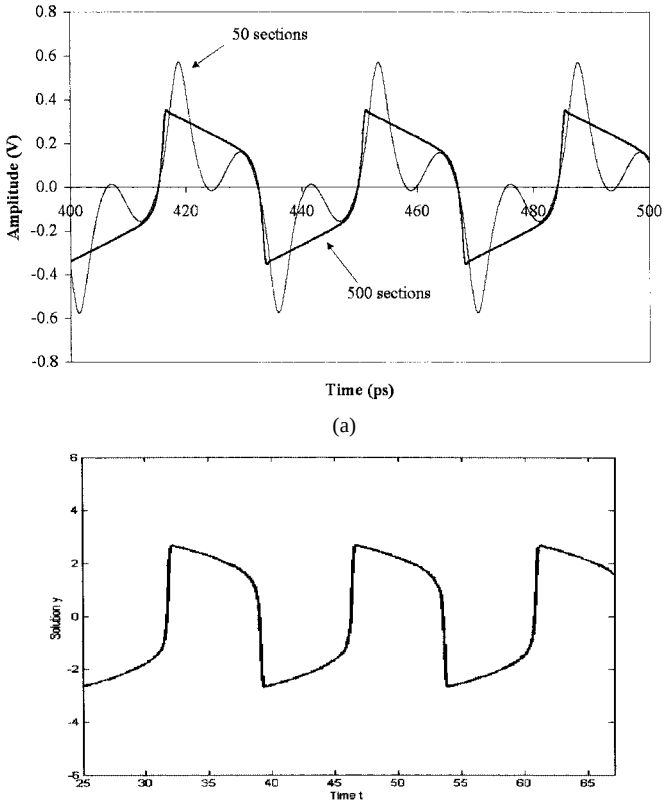

Fig. 5. (a) Simulation of the tripler detailed in [7]. (b) Solution of the GvdP equation with $a = 7$, $b = 4$ (see Appendix II).

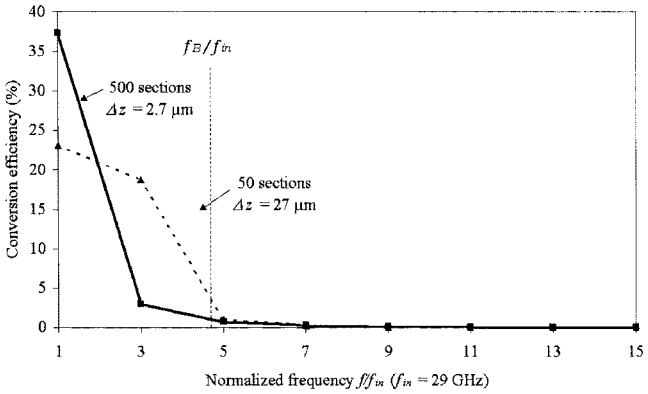

Fig. 6. Harmonic amplitudes corresponding to the waveforms of Fig. 5.

A similar convergence study has been carried out for harmonic generation, considering the magnitude of the third harmonic $3 \cdot f_{\mathrm{in}}$. Fig. 7 shows the amplitude of this harmonic versus the ratio . The fundamental is also shown. This gives an idea of the leakage of power at the fundamental frequency.

The convergence is better than 5% for $f_{B,\mathrm{num}} > 0.3 f_{c,\mathrm{ls}}$, leading to approximately the same condition as was found for pulse compression

$$f_{B,\mathrm{num}} > \frac{f_{c,\mathrm{ls}}}{4}. \quad (4)$$

However, reasonable convergence is still obtained for the condition $f_{B,\mathrm{num}} > f_{c,\mathrm{ls}}/13$, and simulation times can be reduced.

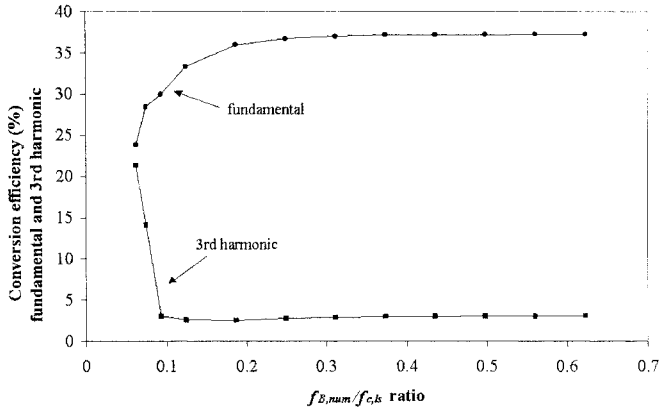

Fig. 7. Amplitude of the fundamental and the third harmonic versus the ratio between the numerical Bragg and physical cutoff frequencies.

B. Application to an HBV Tripler From 20 to 60 GHz

We have simulated both PL and FD NLTLs incorporating the HBVs developed by IEMN [8], using the measured $C(V)$ characteristic of Fig. 1.

1) PL NLTL Tripler Design: For the PL design, the coplanar waveguide (CPW) configuration of Fig. 8 was simulated. Here $Z_{\rm cpw}$ is the characteristic impedance of the linear CPW, τ is the time delay corresponding to one elementary section, represents dc losses in the conductors, is $C(V)$ the voltage-variable capacitance of a single HBV, andR_s is its series resistance. Metallic fingers are used to decrease resistive losses due to the CPW central conductor, as explained by Rodwell *et al.* [1]. Using such fingers, the width W of the central conductor can be increased to reduce dc losses without increasing due to the larger S that would otherwise be needed to maintain a constant CPW characteristic impedance. An electromagnetic study has been carried out to fix the gap (SGap) between the central conductor and the fingers. It is found that if SGap exceeds 5 μm, the gap capacitance is negligible. Therefore, SGap is set to 5 μm in this case.

Four input parameters are needed to determine the electrical model of an elementary section: the Bragg frequency f_B, the small-signal characteristic impedance of the CPW, its large-signal value $Z_{\rm ls}$ (set to a constant 50 Ω), and the number of nonlinear elements N. The Bragg frequency must be chosen to lie between the third and fifth harmonics so that the fifth harmonic is filtered out. In the present case, f_B must lie between 60–100 GHz. The possible domain of variation for $Z_{\rm CPW}$ is 60–120 Ω. The minimum value 60 Ω is imposed by the simultaneous requirements that the large-signal characteristic impedance $Z_{\rm ls}$ should be 50 Ω and that $Z_{\rm cpw}/Z_{\rm ls} = \sqrt{1+C_{\rm ls}/C_{\rm cpw}}$ should exceed unity. The maximum value of $Z_{\rm cpw}(120\ \Omega)$ is fixed by the geometrical limits of CPW technology. For $Z_{\rm cpw} = 120\ \Omega$, we obtain $S = 100\,\mu$m and $W = 5\,\mu$m. The simulation process, which is outlined in Fig. 9, automatically launches SPICE, and then calculates the Fourier transforms and harmonic conversion efficiencies for the variation ranges of the input parameters.

From the three input parameters described above, one can derive all the elements of the equivalent circuit for each NLTL elementary section. The time delay τ for one elementary section is given by

$$\tau = \frac{Z_{\rm ls}}{\pi f b Z_{\rm cpw}}.$$

The CPW conductor dc losses are represented by

$$R{\rm DC} = \rho_{\rm met}\frac{d}{e_{\rm met}W}$$

where $\rho_{\rm met}$ is the resistivity of the CPW central conductor, and $e_{\rm met}$ is its thickness.

The HBV series resistance is given by

$$R_s = R_c + R_d.$$

Here, R_c is the resistance of the ohmic contact between the N_{++} layer and conductor, and R_d is the equivalent series resistance of the N_{++} layer in the gap between the central conductor and metallic fingers, given by

$$R_d = \rho_{n++}\frac{S}{e_{n++}L_{\rm HBV}}$$

in which ρ_{n++} is the N_{++} layer resistivity, and e_{n++} is its thickness. The zero-bias capacitance C_{j0} of the HBV is deduced from the large-signal capacitance $C_{\rm ls}$ calculated by the relation

$$C_{\rm ls} = \frac{\tau}{Z_{\rm cpw}}\left(\frac{Z_{\rm cpw}^2}{Z_{\rm ls}^2}-1\right).$$

Finally, the geometrical parameters are deduced from electrical parameters. Thus, the length of the active area is

$$L_{\rm HBV} = \frac{A}{W}$$

where A is the HBV area, and W is the width of the CPW central conductor. The length of an elementary section is

$$d = \frac{\tau}{\sqrt{\varepsilon r{\rm eff}}}.$$

2) FD NLTL Tripler Design: The design of the FD NLTL is completely different from that of the PL NLTL because no Bragg cutoff frequency is involved. As shown in the flow graph of Fig. 10, the input parameters are mostly geometric.

They consist of three CPW parameters: the conductor width W, gap S, and permittivity ε_r, NLTL length $L_{\rm FD}$, and also relation $f_{B,\rm num} > f_{c,\rm ls}/4$, necessary to avoid any inaccuracies due to a numerical Bragg cutoff frequency.

The first design step is to determine the CPW conductor losses $(R_{{\rm DC}-z})$, characteristic impedance and phase velocity from W, S, and ε_r, knowing the large-signal capacitance $C_{{\rm ls}-z}$ and the series resistance R_{s-z} of the HBV. The section length Δz is calculated such that criterion (4) is satisfied. In the second step, the CPW per-length inductance $L_{{\rm cpw}-z}$ and capacitance C_{jo-z}, the zero-biased HBV capacitance C_{j0-z}, and the large-signal cutoff frequency $f_{c,\rm ls}$ are calculated. In the third step, the NLTL large-signal characteristic impedance $Z_{\rm ls}$, numerical Bragg frequency $f_{B,\rm num}$, and number of sections N used for the simulation are calculated. The CPW dimensions W and S are varied until the best FD NLTL is obtained for realistic dimensions.

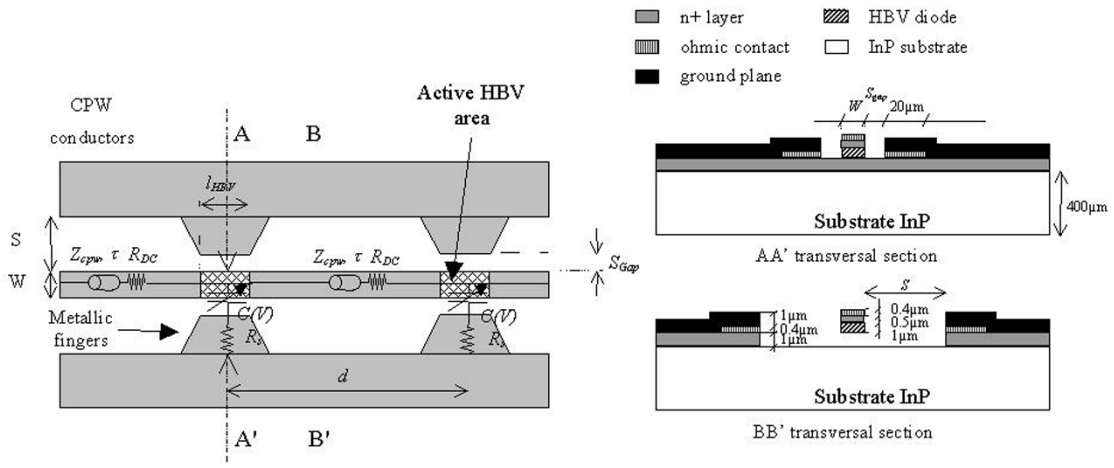

Fig. 8. CPW NLTLs. The electrical equivalent circuit is superimposed.

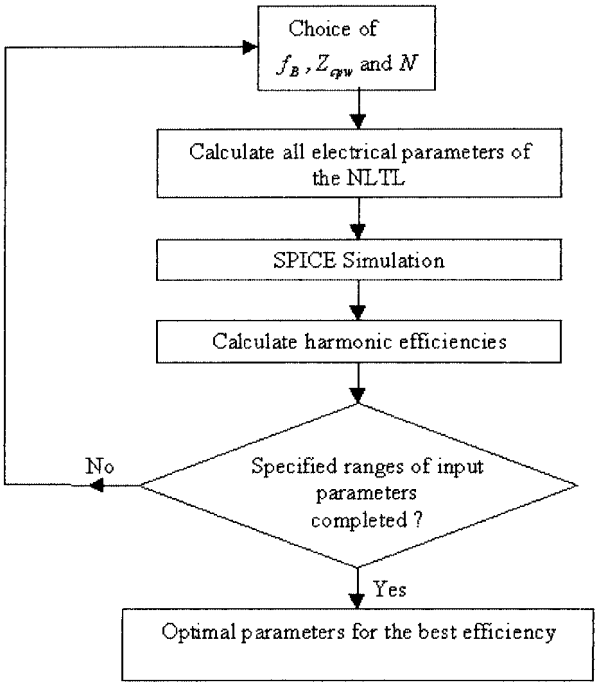

Fig. 9. Optimization procedure for the automatic design of PL NLTLs.

3) Comparison Between PL and FD Tripler Simulation Results: The PL and FD NLTLs were both fed by 20-$V_{\text{peak}-\text{peak}}$ sinewave signals, corresponding to a near-end input power of 1 W. Fig. 11 compares the far-end waveforms of the optimized PL and FD triplers. An efficiency of 21.1% is obtained with the PL structure; in this case, $Z_{\text{cpw}} = 120\,\Omega$, $f_B = 80$ GHz, and $N = 14$ for $Z_{\text{ls}} = 50\,\Omega$. For the FD case, the best efficiency is only 4.8% with $Z_{\text{cpw}} = 95\,\Omega$, $f_{B,\text{num}}/f_{c,\text{ls}} = 4$ leading to $\Delta z = 1.145\,\mu$m (simulation step), and $L_{\text{FD}} = 800\,\mu$m (the length L_{FD} was varied over 100-μm steps).

The electrical and geometrical characteristics of these two NLTLs are summarized in Table I.

For the PL NLTL, the bandwidth reaches 30%, as shown in Fig. 12. This is a very promising result. As shown in Appendix I,

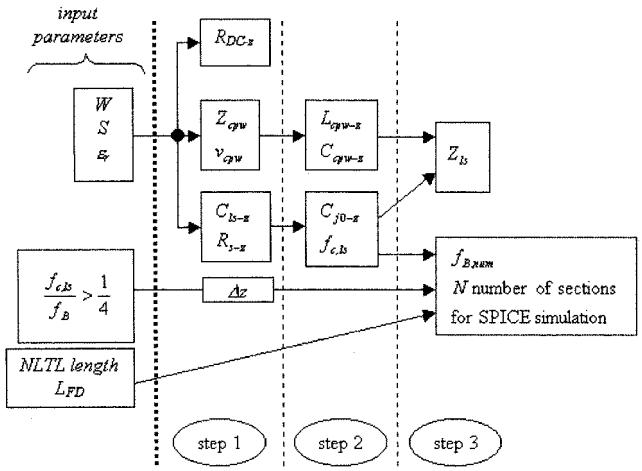

Fig. 10. Design procedure for FD NLTLs. The "$-z$" subscripts indicate per-length electrical parameters.

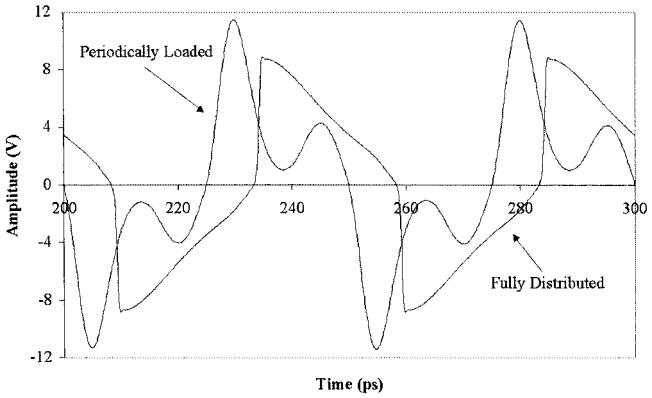

Fig. 11. Triplers simulated with HBVs realized at IEMN.

a tripler realized with a symmetrical $C(V)$ characteristic is the best choice for bandwidth considerations.

In Fig. 12, the fundamental and harmonic five at the NLTL far end have been plotted. They reach 26.8% and 1.6%, respectively, when the third harmonic is maximum. Thus, the total power transmitted to the load approximates 49.4%.

TABLE I
NLTL CHARACTERISTICS

Periodically-Loaded NLTL							
Electrical parameters	$R_{DC} = 0.781\,\Omega$	$R_s = 1.533\,\Omega$	$\tau = 1.658$ ps	$C_{j0} = 169$fF	$C_{ls} = 65.8$ fF		
Geometrical parameters	$W = 5\,\mu$m	$S = 100\,\mu$m	$d = 195\,\mu$m	$l_{HBV} = 32.9\,\mu$m	$A = 164\,\mu$m^2	$N = 14$	$L_{PL} = 2.73$ mm
Fully-Distributed NLTL							
Electrical parameters	$R_{DC} = 6.7$ mΩ/μm	$R_s = 62.5\,\Omega/\mu$m	$C_{j0} = 3$ fF/μm	$C_{ls} = 1.17$ fF/μm			
Geometrical parameters	$W = 3\mu$m	$S = 20\,\mu$m	$L_{FD} = 800\,\mu$m				

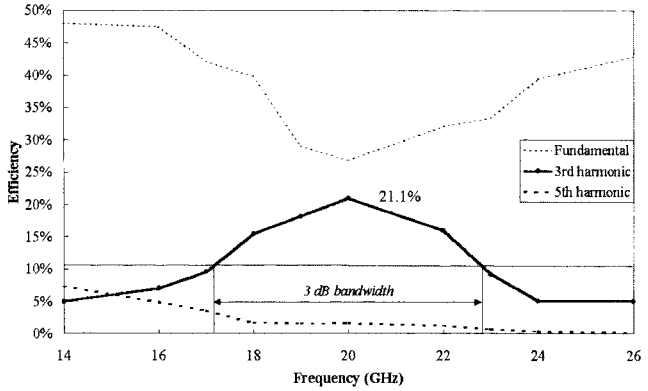

Fig. 12. Bandwidth of the PL NLTL tripler.

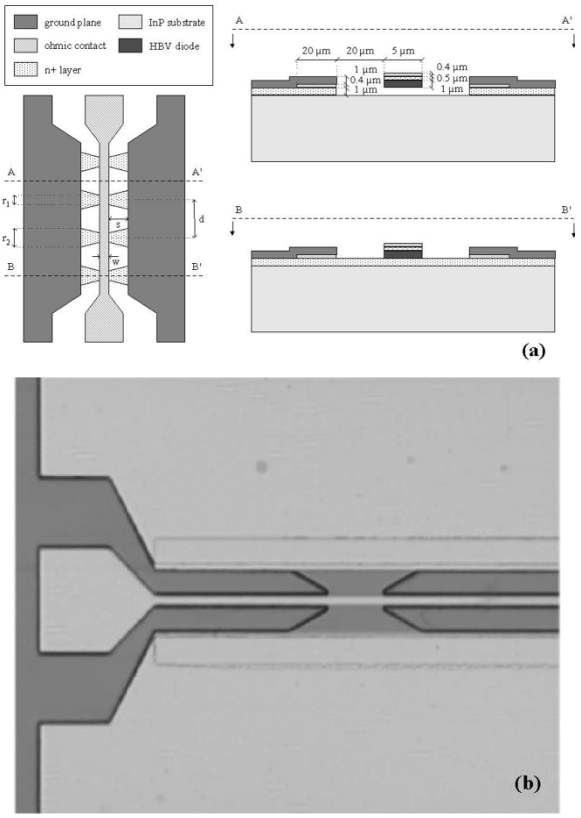

Fig. 13. (a) Illustration of technology employed for the tripler prototype. (b) Optical view of the PL prototype.

For the FD NLTL, the best efficiency is obtained with $Z_{\rm ls} = 25\,\Omega$. The NLTL is not matched to 50 Ω if the goal is to obtain the best efficiency. This confirms Rodwell's remarks [6]. Unlike the PL NLTLs, for which an increase of W (decrease of metallic losses) leads to an improved third harmonic efficiency if metallic fingers are used to connect the diodes, W must be decreased in the case of FD NLTLs. For FD NLTLs, if W is increased, S must be increased in order to leave the CPW characteristic impedance unchanged. The increase of S leads to an increase of the HBV series resistance R_s. Simulations show that W must be very small. In our case, a limit of 3 μm was imposed by the technology. If W is increased without increasing S, $Z_{\rm ls}$ decreases, leading to a decrease of $Z_{\rm ls}$, and then a mismatched NLTL. Too large a mismatch would reduce the efficiency. Simulation results simply show that a tradeoff exists between a diminishing S and an excessive mismatch. In the case of the NLTLs designed in this paper, this leads to $Z_{\rm ls} = 25\,\Omega$

With respect to the self-heating effect, which results from an increase in temperature and, hence, of the leakage current for poor conversion operation, it seems that special care has to be paid to the thermal management. On this basis, a FD may exhibit a better thermal conductivity with respect to the PL counterpart. However, it has to be emphasized that, in the present InP technology, these effects will only affect the diode performances under very hard pumping conditions. Let us recall the very low leakage current resulting from a very high conduction band offset at the heterointerfaces between the cladding layers and blocking barrier.

4) Experimental PL NLTL Verification: The theoretical analysis predicts a PL NLTL with both wide bandwidth and high efficiency. To validate this prediction, we fabricated a prototype in a coplanar technology. Starting with an InP semi-insulating substrate, we grew two integrated heterostructure barrier varactors in series in order to increase voltage handling and impedance level through a decrease in overall capacitance. Variation of the depletion region occurs in InGaAs cladding layers, whereas the blocking barrier consists of an InAlAs/AlAs/InAlAs tri-layer. The PL NLTL prototype was fabricated as shown in the two cross sections of Fig. 13(a). The main difference between this layout and the one in Fig. 8 is the use of a different contact layer. In Fig. 13(a), the slot width is kept constant at 20 μm, while the strip width is 5 μm. The contact to the side metallization is via the highly doped buried InGaAs layers, and a trapezoidal contact shape minimizes the series resistance. Isolation between diodes is obtained by underetching. Fig. 13(b) shows a close-up optical view

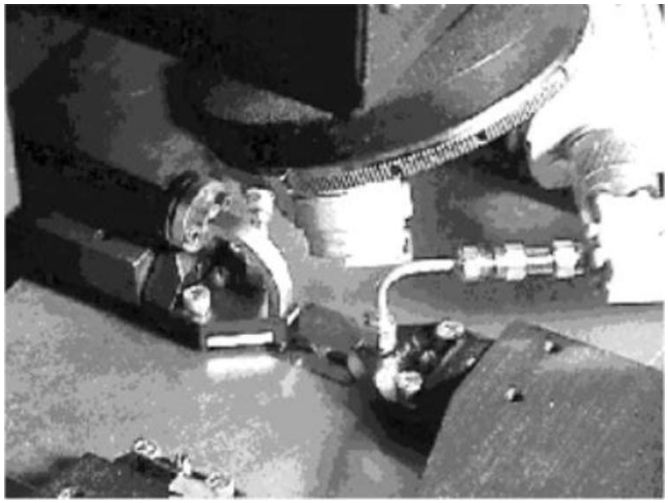

Fig. 14. Measurements probe setup.

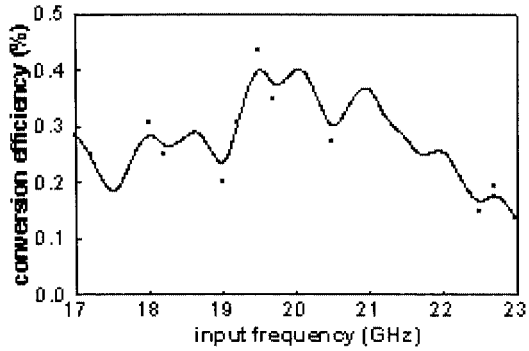

Fig. 15. Frequency response, data (dots), and smoothed interpolation (line).

illustrating the contact layers. It also shows the tapered region provided to facilitate conventional wafer probing.

For the measurements, we use the probe setup depicted in Fig. 14. Here, the input section is fed by a coaxial transmission line, while the waveguide output section is designed for operation at V-band (50–75 GHz). Consequently, there exists a waveguide cutoff that was not been included in the previous analysis. Since the epitaxial material has two barriers in series to improve both voltage and power handling, high-level diode pumping is needed for a full C–V excursion. Here, the pumping source consists of a vector-network-analyzer synthesizer followed by an amplifier. Since the effective diode impedance depends on the signal voltage, the impedance matching is not optimal. Finally, we believe that the series resistance R_s for the prototype of Fig. 13(a) is larger than that for Fig. 8. The total resistance also depends on the number of diodes along the line (eight here). Consequently, this prototype could not achieve the 21% efficiency predicted for an optimized 14-section structure.

On the other hand, the measurements do validate the bandwidth calculations. This can be seen from Fig. 15, which shows the measured conversion efficiency versus input frequency under moderate power pumping conditions. Some ripple, attributable to interference effects due to spurious reflections, is seen in the response between 17–23 GHz.

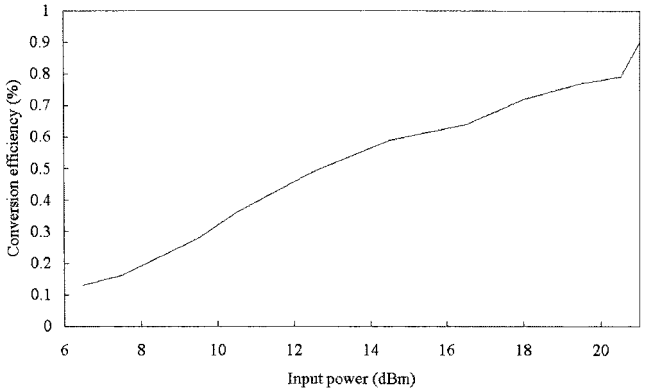

Fig. 16. Conversion efficiency versus input power.

Nevertheless, the 3-dB bandwidth of ∼30% is in good agreement with calculation. Fig. 16 shows the measured conversion efficiency versus the input power.

With an input power of 21 dBm, the conversion efficiency reaches 0.9%. This is in good agreement with both SPICE and harmonic-balance simulations of this prototype, originally designed for an input power of 30 dBm.

C. Application to the Compression of a 16-ps Pulse

When HBVs are used as nonlinear elements for pulse compression, only one-half of the $C(V)$ characteristic is used. The main reasons for using HBVs rather than Schottky diodes are the possibilities of higher breakdown voltage and tailoring the $C(V)$ shape. In this investigation, the NLTLs were not specifically optimized for pulse compression; the parameters given in Table I have been used. The large-signal characteristic impedance $Z_{\rm ls}$ of the NLTL is never equal to 50 Ω. For dc biases of 5 and 10 V, $Z_{\rm ls} = 21.9$ and $25\,\Omega$, respectively. To bring to the fore the importance of the mismatch between and the load and source impedances, two sets of simulations were carried out for FD NLTLs, first using 50-Ω source and load impedances, meaning that the NLTL is strongly mismatched and, second, with the source and load impedances made equal to $Z_{\rm ls}$.

For the first set of simulations, the NLTLs are biased at 5 V and fed by a pulse generator delivering a 10-V pulse with a 10%–90% rise time of 16 ps. Fig. 17 shows the simulation results for 50-Ω source and load impedances when the NLTL length $L_{\rm FD}$ is varied from 800 to 1600 μm in 200-μm steps.

For the PL NLTL, the far-end rise time is 5.3 ps, but for the FD NLTL, the rise time is only 1.8 ps when full compression is achieved ($L_{\rm FD} = 1600\ \mu$m). Thus, the FD design gives a better compression result than the PL design. Moreover, no overshoot occurs for the FD NLTL in the absence of a Bragg cutoff frequency. Fig. 17 clearly shows the mismatch of the FD NLTLs: there is a reflection between 90–150 ps depending on the NLTL length.

Simulation results for matched FD NLTLs are given in Figs. 18 and 19. The NLTLs are dc biased at 5 and 10 V, respectively. The simulated far-end rise times are very small, being 1.03 and 0.64 ps. The 10-V biased NLTL gives the best

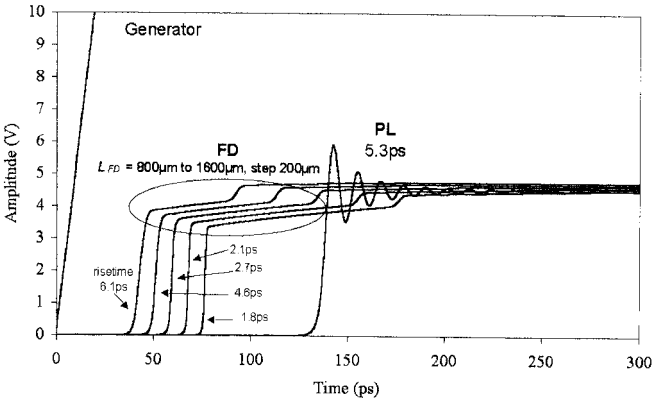

Fig. 17. Output pulses for the FD NLTLs fed by a 10-V pulse generator. Source and load impedances are fixed at 50 Ω.

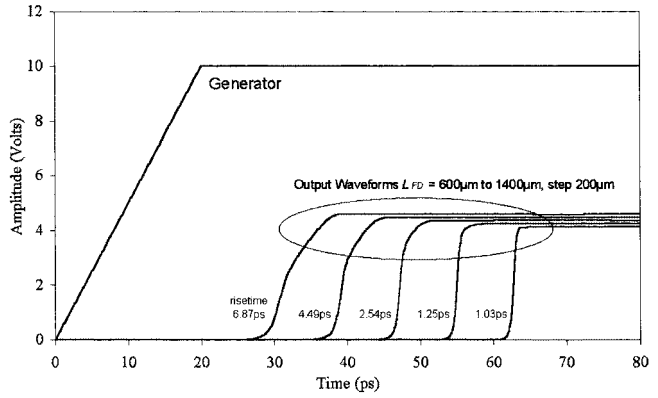

Fig. 18. Output pulses for the FD NLTLs fed by a 10-V pulse generator. Source and load impedances are fixed at 21.9 Ω so that the NLTLs are matched.

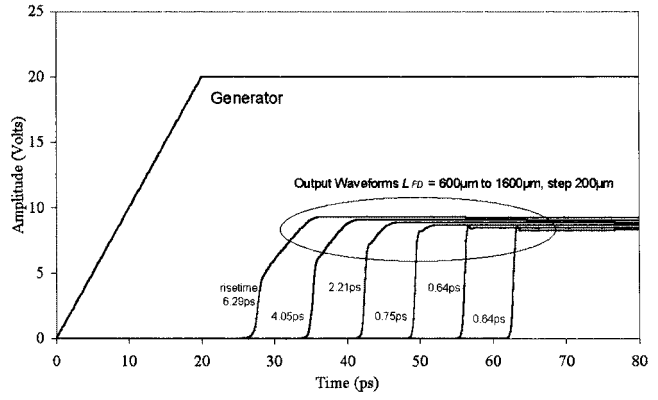

Fig. 19. Output pulses for the FD NLTLs fed by a 20-V pulse generator. Source and load impedances are fixed at 25 Ω so that NLTLs are matched.

performance because the diode $C_{\max}/C_{\min}$ ratio is larger, leading to a much better compression efficiency [1]. The NLTL length necessary to obtain full compression does not depend on the dc bias voltage; it is found that $L_{\rm FD} \sim 1400\,\mu$m for either 5- or 10-V bias.

These results are interesting and suggest that further investigations of FD NLTLs should be undertaken. To go further, skin-effect losses inside the semiconductor need to be accurately modeled and taken into account in the simulations. Skin-effect losses can be taken into account in SPICE simulations, as shown in [10]. Also, source and load impedances different from 50 Ω can really be a problem for pulse compression applications. Perhaps a technology other than the CPW should be used, such as finline, for example, in order to achieve optimal compression for 50-Ω impedances.

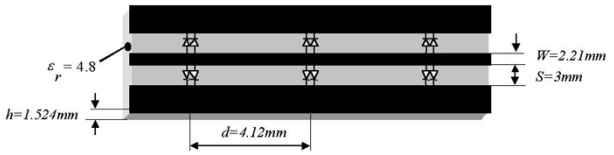

Fig. 20. Hybrid Schottky PL NLTL frequency multiplier with $N = 5$ sections (only three are represented).

For pulse-compression applications, it is important to minimize the skin-effect losses caused by unwanted longitudinal currents flowing in the low-doped HBV regions. A possible way to do this is to subdivide the "continuous" HBV part of the NLTL structure into a sequence of short semiconductor sections interspersed by thin insulating sections. This would have little effect on the effective per-length R_s of the quasi-distributed HBV, but would inhibit the flow of longitudinal currents and, hence, the associated losses. The analogy here is the use of laminated iron cores in low-frequency transformers to reduce eddy-current losses. The subdivision would, of course, introduce a Bragg cutoff at a frequency determined by the smallest feature size the process can accommodate. Thus, we are led to the idea of optimizing a pulse-compression NLTL by "loading an NLTL with linear elements." This can be thought of as the dual of optimizing a frequency-multiplying NLTL by "loading a linear transmission with nonlinear elements."

IV. Realization of FD-PL Hybrid Schottky NLTLS

This section provides experimental results that verify the theoretical conclusions concerning the influence of the geometrical discretization length d in the PL NLTLs (see Fig. 7) on the multiplier efficiency.

A. Rationale for Hybrid Schottky NLTL Multipliers

In the present experimental part of this study, it was not possible to fabricate high-frequency monolithic multipliers such as those characterized in Section III-B in a systematic fashion. Therefore, we have realized a hybrid Schottky-diode PL NLTL. With these structures, we can confirm the conclusions concerning harmonic generation that were derived from the simulation results of Section III.

B. Results

A hybrid Schottky-diode PL NLTL was optimized for maximum conversion efficiency to the second harmonic at 480 MHz. It was realized on an Epoxyed resin (FR3) substrate. All dimensions and characteristics are given in Fig. 20; there are $N = 5$ sections, and the CPW characteristic impedance is 91 Ω.

The Schottky diode is an hyperabrupt GaAs device from Agilent Technologies, Massy, France. The classical equivalent-cir-

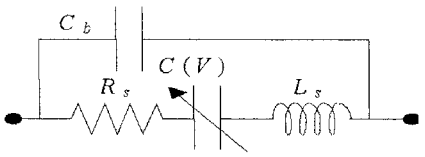

Fig. 21. Schottky diode electrical equivalent model.

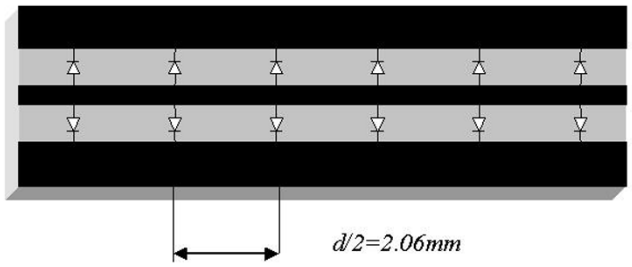

Fig. 22. Quasi-distributed hybrid NLTL frequency multiplier with $N = 10$ sections (only six are represented).

cuit model used for the simulations is given in Fig. 21. The reverse-biased nonlinear capacitance is expressed as

$$C(V) = \frac{C_{j0}}{\left(1 + \frac{V}{V_{j0}}\right)^M} \tag{5}$$

and we used the manufacturer values $C_{jo} = 3.55$ pF, $M = 0.75$, $V_{jo} = 0.7$ V, $R_s = 4\,\Omega$, $L_s = 500$ pH, and $C_b = 130$ fF

We can obtain a "more distributed" nonlinearity by simultaneously reducing the length of the elementary sections and reducing the number of diodes per section.

With this in mind, we realized a second NLTL on the same CPW with the same diodes, but having half-length elementary sections, with two diodes per section. This resulted in a ten-section "quasi-distributed" NLTL (see Fig. 22).

The agreement between measurements and simulations in the time domain is good. Measurements validate the simulation model and method. On the waveforms, we can see more high-order harmonics appear for the "distributed" NLTL than on the five section one. This is confirmed by taking the Fourier transforms of Fig. 23 waveforms. Fig. 24 shows the conversion efficiency for harmonics h_2, h_3, and h_4 (corresponding to 960, 1240, and 1720 MHz), generated by these two NLTLs, versus the ratio between the Bragg frequency and the large-signal cutoff frequency defined by (3). The large-signal cutoff frequency is that obtained for the simulations.

Again, the agreement between the measurements and simulations is good. What is important is the decreased second-harmonic (h_2) conversion efficiency for the quasi-distributed NLTL, and the increased third-harmonic (h_3) efficiency. Even though we deal here with hybrid Schottky NLTLs rather than integrated HBV NLTLs, the similarity between these results and those simulated for the HBV tripler (see Fig. 7) is quite clear.

When the NLTL nonlinearity is distributed and the Bragg cutoff no longer acts as a low-pass filter, the power is spread

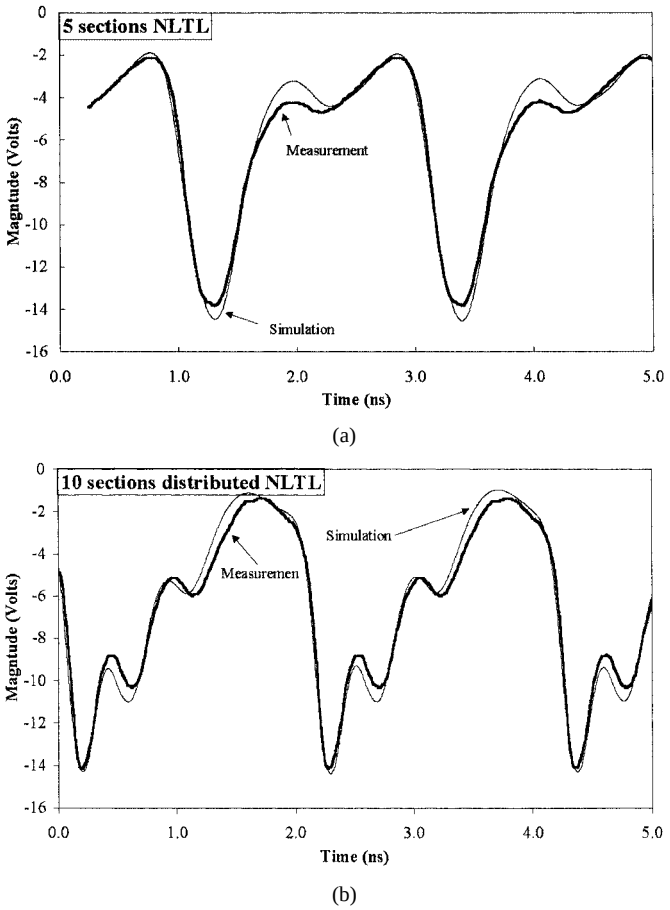

Fig. 23. Comparison between measured results and SPICE simulations for: (a) the hybrid PL NLTL and (b) the "quasi-distributed" hybrid NLTLs.

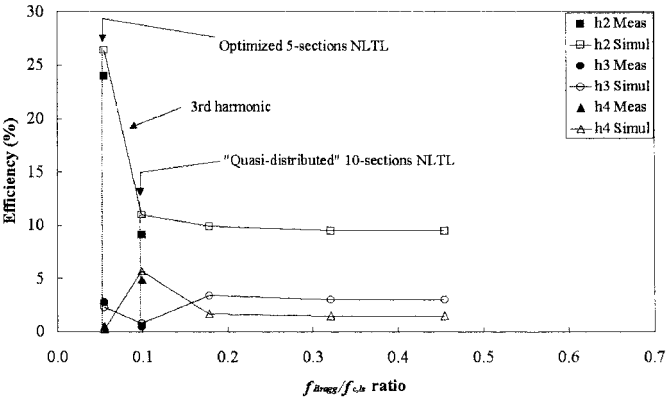

Fig. 24. Conversion efficiency for second (h_2), third (h_3), and fourth (h_4) harmonics versus the ratio between the Bragg frequency and the large-signal cutoff frequency.

over high-order harmonics and the conversion efficiency to the first harmonic is decreased compared with a PL NLTL. This confirms the early results of Jäger and Tegude [11] concerning a microstrip FD NLTL realized on silicon. They obtained 1% efficiency at room temperature and 2% at $T = 77$ K and concluded "Yet it is nevertheless difficult to imagine practical applications of the presented SCMLs" and foresaw the realization of PL NLTLs to "prevent generation and flow of undesired harmonics" [12].

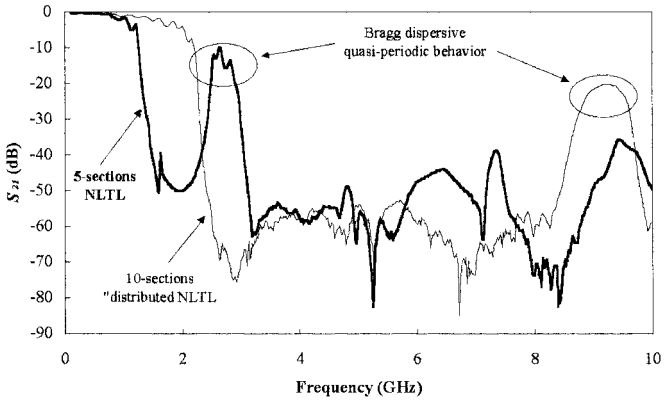

Fig. 25. Measured modulus of S_{21} for the two NLTLs when biased at -6 V.

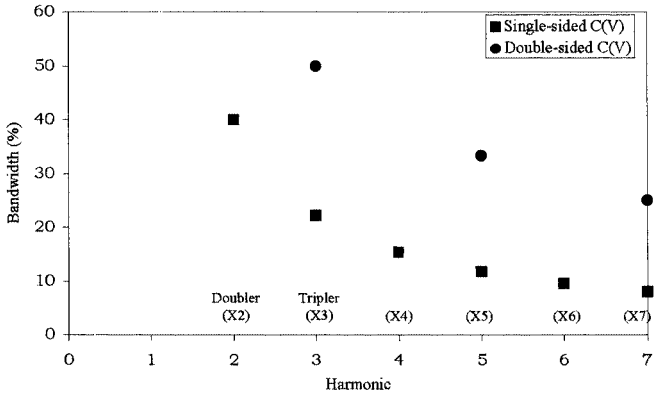

Fig. 26. Comparison of the best theoretical bandwidths for single- and double-sided $C(V)$ characteristics.

To go further, it is interesting to experimentally estimate the Bragg frequency for the two NLTLs. The Bragg frequency cannot be rigorously measured, but we can obtain a good approximation from small-signal measurements using a vector network analyzer [13]. Fig. 25 shows the measured modulus of S_{21} for the two NLTLs when biased at -6 V. We see that rapidly decreases for frequencies above 1200 and 2200 MHz, respectively. We also note the quasi-periodic behavior of the Bragg dispersion.

We also determined an experimental value for the optimal input frequency for maximum second harmonic (h_2) generation with the quasi-distributed NLTL. We obtained 31% conversion efficiency at 760 MHz. This is better than the 24.5% obtained for the PL NLTL fed at 480 MHz; however, this is not surprising since the number of sections is ten instead of five. This result was confirmed by simulations.

V. Conclusion

We have carefully compared HBV-NLTLs based on FD and PL approaches for pulse compression and for third harmonic generation. The importance of the choice of simulation step size in the case of FD NLTLs has been pointed out. For the optimized triplers considered in this paper, a 21% efficiency at 210-mW output power and 30% bandwidth is expected in practice for the PL approach, compared with a 4.8% efficiency and 48-mW output for the FD case. The 30% FD bandwidth has been confirmed experimentally.

Measurements on hybrid Schottky-based multipliers confirm the importance of the Bragg cutoff effect in preventing the generation and propagation of undesired high-order harmonics by acting as a low-pass filter.

For pulse compression, the NLTL far-end rise time is very similar in the two cases when the large-signal characteristic impedance $Z_{\rm ls}$ is fixed at 50 Ω, although the FD NLTL is strongly mismatched and significant reflections occur at its far end. If we work with $Z_{\rm ls}$ values different from 50 Ω, much sharper pulses can be obtained with FD NLTLs, the far-end rise time $(<1$ ps$)$ being reduced by a factor of $\sim$5. To go further, skin-effect losses in the semiconductor need to be carefully modeled and introduced into the simulation models to ensure that FD NLTLs are viable for pulse compression applications.

Appendix I
Best Theoretical Multiplier Bandwidth

We define the "best theoretical bandwidth" as the bandwidth imposed by the Bragg filtering effect. For a frequency doubler using a single-sided $C(V)$ characteristic, realized, for example, with Schottky diodes, the input frequency $f_{\rm in}$ must be set between $f_B/2$ and $f_B/3$, i.e., $f_B/3 < f_{\rm in} < f_B/2$. If $f_{\rm in}$ is below $f_B/3$, then significant third harmonic power will appear at the NLTL far end and consume power, decreasing the second-harmonic conversion efficiency [11]. If $f_{\rm in}$ is greater than $f_B/2$, then the Bragg cutoff frequency will prevent second harmonic generation. The single-sided bandwidth $\mathrm{BW}_{\rm ss}$ is

$$\mathrm{BW}_{\rm ss} = \frac{\frac{f_B}{2} - \frac{f_B}{3}}{f_0} = \frac{2}{5} \equiv 40\%$$

where $f_0 = (f_B/2 + f_B/3)/2$ is the arithmetic center frequency.

For a tripler employing a double-sided symmetrical $C(V)$ characteristic, for example, using HBVs, the same analysis shows that the input frequency $f_{\rm in}$ must be set between $f_B/3$ and $f_B/5$, i.e., $f_B/5 < f_{\rm in} < f_B/3$. We find that the double-sideband bandwidth $\mathrm{BW}_{\rm ds}$ is

$$\mathrm{BW}_{\rm ds} = \frac{f_B}{3} - \frac{\frac{f_B}{5}}{\frac{f_B}{3}} + \frac{f_B}{5} \cdot 2 = \frac{1}{2} \equiv 50\%.$$

Generalizing the bandwidth equations, we find that $\mathrm{BW}_{\rm ss} = 2/(4k+1)$ and $\mathrm{BW}_{\rm ds} = 1/(k+1)$, where k is the harmonic range (Fig. 26).

Appendix II
Comments on the FD NLTL Tripler Waveform

As mentioned in Section III-A, the tripler of [7] produces a "sawtooth" waveform [see Fig. 5(a)] that is remarkably similar to the solution of a GvdP equation with suitably chosen coefficients [see Fig. 5(b)]. What is interesting is that both waveforms are generated by purely cubic nonlinearities. In the case of the

FD NLTL of [7], the waveform is produced by a partial derivative wave equation of the form

$$\frac{\partial^2}{\partial z^2}(x+\beta x^3)+\xi\frac{\partial^3 x}{\partial z^2\partial t}=\frac{1}{u^2}\frac{\partial^2 x}{\partial t^2}$$

where x is the normalized charge/length of the distributed HBV structure, z is the distance along the NLTL, t is the time, u is a phase velocity, β is a constant HBV capacitance-related parameter, and ξ is a loss parameter. In the case considered, $\beta = 3.0$. Here, the cubic is of the form

$$f(x) = x + \beta x^3.$$

The waveform in Fig. 5(b) is the solution of the generalized van der Pol (GvdP) oscillator equation. Its ordinary differential equations (ODEs)

$$\frac{d^2y}{dt^2}-\frac{d}{dt}(ay-by^3)+y=0$$

using $a = 7$, $b = 4$. Here, the cubic is

$$f(y) = -ay + by$$

and the solution was obtained using the "ode15s" stiff ODE solver of Matlab Release 12.

It is conjectured that the FD NLTL of [7] can be thought of as being related to an "unrolled" GvdP oscillator. In the former case, the sawtooth waveform is built up over space (the length of the NLTL), in the latter case, the sawtooth waveform is built up over time (the oscillator regeneration process).

REFERENCES

[1] M. J. Rodwell, S. T. Allen, R. Y. Yu, M. G. Case, U. Bhattacharya, M. Reddy, E. Carman, M. Kamegawa, Y. Konishi, J. Pusl, and R. Pullela, "Active and nonlinear wave propagation in ultrafast electronics and optoelectronics," *Proc. IEEE*, vol. 82, pp. 1037–1059, July 1994.

[2] D. Jäger, "Pulse generation and compression on nonlinear transmission lines," in *IEEE MTT-S Int. Microwave Symp. Dig.*, 1993, pp. 37–57.

[3] H. Shi, W.-M. Zhang, C. W. Domier, N. C. Luhman, Jr., L. B. Sjogren, and H.-X. L. Liu, "Novel concepts for improved nonlinear transmission line performance," *IEEE Trans. Microwave Theory Tech.*, vol. 43, pp. 780–789, Apr. 1995.

[4] S. Hollung, J. Stake, L. Dillner, M. Ingvarson, and E. Kollberg, "A distributed heterostructure-barrier varactor frequency tripler," *IEEE Microwave Guided Wave Lett.*, vol. 10, pp. 24–26, Jan. 2000.

[5] K. Everszumrode, B. Brockman, and D. Jäger, "Efficiency of harmonic frequency generation along Schottky contact microstrip lines," *Arch. Elektron. Uebertrag. Tech.*, vol. 31, pp. 212–215, May 1977.

[6] M. J. W. Rodwell, "Picosecond electrical wavefront generation and picosecond optoelectronic instrumentation," Ph.D. dissertation, Stanford Univ., Stanford, CA, 1987.

[7] M. Li, K. Krishnamurthi, and R. G. Harrison, "A fully distributed heterostructure-barrier-varactor nonlinear transmission line frequency multiplier and pulse sharpener," *IEEE Trans. Microwave Theory Tech.*, vol. 46, pp. 2295–2301, Dec. 1998.

[8] X. Mélique, A. Maestrini, P. Mounaix, M. Favreau, O. Vanbésien, J. M. Goutoule, G. Beaudin, T. Närhi, and D. Lippens, "Record performance of a 250 GHz InP-based heterostructure barrier varactor tripler," *Electron. Lett.*, vol. 35, no. 11, pp. 938–939, May 1999.

[9] M. Fernandez, E. Delos, X. Mélique, S. Arscott, and D. Lippens, "Monolithic coplanar transmission lines loaded by heterostructure barrier varactors for a 60 GHz tripler," *IEEE Microwave Wireless Comp. Lett.*, vol. 11, pp. 498–500, Dec. 2001.

[10] A. Jrad, W. Thiel, P. Ferrari, and J. W. Tao, "Comparison of SPICE and FDTD simulations for lossy and dispersive nonlinear transmission lines," *Electron. Lett.*, vol. 36, no. 9, pp. 797–798, May 2000.

[11] D. Jäger and F. J. Tegude, "Nonlinear wave propagation along periodic-loaded transmission lines," *Appl. Phys.*, vol. 15, pp. 393–397, 1978.

[12] J. Becker, D. Jäger, and W. Schäfer, "DC-tunable stripline-filters with low-pass characteristic," *Arch. Elektron. Uebertrag. Tech.*, vol. 31, pp. 77–80, May 1977.

[13] M. F. Diego, "Non linear transmission line for frequency multiplier applications," Ph.D. dissertation, Dept. Electron., Univ. Lille, Lille, France, 2001.

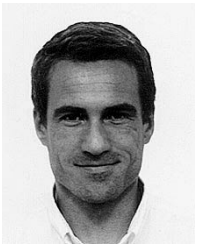

Jean-Marc Duchamp was born in Lyon, France, on April 10, 1965. He received the M.Sc. and Supelec Ingeneer degrees from the University of Orsay, Orsay, France, in 1988 and 1990, respectively, and is currently working toward the Ph.D. degree at the Université de Savoie, Savoie, France.

From 1991 to 1996, he was a Research Engineer. He currently teaches electronics at the Université de Savoie. His current research interests include nonlinear microwave and millimeter-wave circuits analysis and design.

Philippe Ferrari was born in France, in 1966. He received the B.Sc. degree in electrical engineering and Ph.D. degree from the Institut National Polytechnique de Grenoble (INPG), Grenoble, France, in 1988 and 1992, respectively.

In 1992, he joined the Laboratory of Microwaves and Characterization, Université de Savoy, Bourget-du-lac Cedex, France, where he is currently an Assistant Professor in electrical engineering. He is currently the Head of the laboratory project on NLTLs. His main research interest is the conception and realization of NLTLs for the generation and measurement of ultra-fast microwave signals and frequency multipliers. He is also involved in the development of time-domain techniques for the measurement of passive microwave devices and soil moisture content.

M. Fernandez, photograph and biography not available at time of publication.

A. Jrad, photograph and biography not available at time of publication.

Xavier Mélique was born in Tourcoing, France, on April 12, 1972. He received the M.S. and Ph.D. degrees from the Université de Sciences et Technologies de Lille, Lille, France, in 1994 and 1999, respectively.

He is currently an Assistant Professor with the Institut d'Electronique de Microélectronique et de Nanotechnologie (IEMN), Villeneuve d'Ascq, France. His main research interests concern the development of advanced techniques aimed at the planar integration of high-performance III–V heterostructure devices. Up and down frequency conversion at terahertz frequencies with highly nonlinear semiconductor heterostructure devices are the main targeted applications.

Junwu Tao was born in Hubei, China, in 1962. He received the B.Sc. degree in electronics from the Huazhong (Central China) University of Science and Technology, Wuhan, China, in 1982, the Ph.D. degree (with honors) from the Institut National Polytechnique of Toulouse, Toulouse, France, in 1988, and the Habilitation degree from the Université de Savoie, Savoie, France, in 1999.

From 1983 to 1991, he was with the Electronics Laboratory, ENSEEIHT, Toulouse, France, where he was involved with the application of various numerical methods to two- and three-dimensional problems in electromagnetics and the design of microwave and millimeter-wave device. From 1991 to 2001, he was with the Microwave Laboratory (LAHC), University of Savoie, where he was an Associate Professor of electrical engineering and involved in the full-wave characterization of discontinuity in various planar waveguides and the nonlinear transmission-line design. Since September 2001, he has been a Full Professor with the Institut National Polytechnique of Toulouse, where he is involved in the numerical methods for electromagnetics, microwave and RF component design, and microwave and millimeter-wave measurements.

S. Arscott, photograph and biography not available at time of publication.

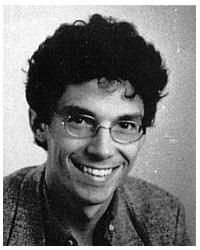

Didier Lippens was born in 1952. He received the Ph.D. and Doctorat d'état degrees in 1978 and 1984, respectively.

He currently heads the Quantum Opto and Micro Electronic Device Group (DOME), Institut d'Electronique de Microélectronique et de Nanotechnologie (IEMN), Université des Sciences et Technologies de Lille, Lille, France. From 1979 to 1980, he was a Research Engineer with Thomson CSF. Since 1989, he has been a Research Director and a Professor with the Université des Sciences et Technologies de Lille, where his main interests concern the development of high-speed devices used in terahertz microelectronics, optoelectronics and photonics with microtechnologies and nanotechnologies as a common denominator.

Dr. Lippins is a member of the Steering Committees of the Network on Nano and Micro-Technologies (RMNT) and of the National Research Network on Telecommunications (RNRT). He is the French corresponding member of the Training Mobility Research (project Interaction) and of the Future Emergent Technology project "Wanted." He is the member of several program committees of terahertz and integrated circuit conferences, held in Europe and Japan, and was the chairman of the III–V Microelectronics and Optoelectronics Conference, Aussois, France, 2001.

R. G. Harrison (M'82) received the B.A. and M.A. (Eng.) degrees from Cambridge University, Cambridge, U.K., in 1956 and 1960, respectively, and the Ph.D. and D.I.C. degrees from the University of London, London, U.K., in 1964.

From 1964 to 1976, he was with the Research Laboratories, RCA Ltd., Ste-Anne-de-Bellevue, QC, Canada. In 1977, he became Director of Research with Com Dev Ltd., where he was involved with nonlinear microwave networks. From 1979 to 1980, he designed spread-spectrum systems with the Canadian Marconi Company, Montreal, QC, Canada. Since 1980, he has been a Professor with the Department of Electronics, Carleton University, Ottawa, ON, Canada. His research interests include the modeling of nonlinear microwave device/circuit interactions by a combination of analytical and numerical techniques and, more recently, the development of analytical models of ferromagnetic phenomena. He has authored or coauthored over 58 technical papers, mostly in the area of nonlinear microwave circuits, as well as several book chapters on microwave solid-state circuit design. He holds a number of basic patents in the area of microwave frequency-division devices.

Dr. Harrison was the recipient of the 1978 Inventor Award presented by Canadian Patents and Development.